Top Catal (2011) 54:737–745
DOI 10.1007/s11244-011-9678-x

ORIGINAL PAPER

Aerobic Oxidation of Cyclohexane Catalyzed by Flame-Made Nano-Structured Co/SiO_2 Materials

Natascia Turrà · Andrea Blanco Acuña · Björn Schimmöller · Bernhard Mayr-Schmölzer · Philipp Mania · Ive Hermans

Published online: 30 April 2011

Abstract The aerobic oxidation of cyclohexane was studied at 130 °C in the presence of a Co/SiO_2 catalyst, synthesized by flame-spray pyrolysis. Characterization of the material indicates that at low Co-loadings, Co^{II} is predominantly present as tetrahedral species, whereas at higher loadings also small amounts of octahedral species can be found at the surface of the agglomerated nanoparticles. Catalytic experiments demonstrate high activity, causing a complete in situ deperoxidation of the intermediate cyclohexylhydroperoxide. Hot-separation and catalyst-recycle tests corroborate the heterogeneous nature of the catalyst.

Keywords Autoxidation · Radicals · Selectivity · Flame-spray-pyrolysis

1 Introduction

The aerobic oxidation of cyclohexane is the most important industrial route to cyclohexanol and cyclohexanone ("KA-oil", 6×10^6 t/y), key intermediates in the production of Nylon-6 and Nylon-6,6 [1]. This reaction is usually performed in bubble column reactors at 140–180 °C [2, 3], with optimized heat integration, i.e., the exothermicity of the reaction is converted into steam, a valuable energy carrier in an industrial network. The conversion is limited to approximately 5% in order to prevent over-oxidation of the desired products, cyclohexylhydroperoxide (CyOOH), cyclohexanol (CyOH) and cyclohexanone (Q=O). Subsequently, the CyOOH product is decomposed to additional CyOH and Q=O in a separate deperoxidation process using a soluble cobalt catalyst such as cobalt(II)octoate. In some cases, a small amount of cobalt is already added during the autoxidation itself, depending on the company [4].

Whereas it was known for a long time that this reaction takes place via radical intermediates such as peroxyl and alkoxyl radicals, it was only recently, that the origin of the products and by-products was detailed [5–7]. Briefly summarized, CyOOH is the pivotal reaction intermediate, produced upon reaction of peroxyl radicals ($CyOO^{\bullet}$) with the cyclohexane substrate, but also consumed upon reaction with $CyOO^{\bullet}$ radicals. The latter reaction yields Q=O—directly—and CyOH—in an activated liquid-phase-induced cage-reaction—as well as a sizable amount of alkoxyl radicals. These $CyO^{\bullet}$ radicals are partially converted to additional alcohol, and partially to ring-opened by-products upon a β-cleavage [6]. Indeed, the majority of by-products originate from this hitherto overlooked co-oxidation of the CyOOH intermediate, and not via over-oxidation of the Q=O products as was assumed before [8].

If catalytic amounts of cobalt ions are present, the Co-ions take over the role of $CyOO^{\bullet}$ radicals in the consumption of CyOOH [9]. Although the mechanism of this reaction is still poorly understood, it is generally assumed that a Haber–Weiss mechanism takes place between the hydroperoxide and the cobalt ions, causing an overall

Dedicated to the 80th birthday of Prof. Dr. Robert K. Grasselli.

N. Turrà · A. B. Acuña · B. Mayr-Schmölzer · P. Mania · I. Hermans (✉)
Department of Chemistry and Applied Biosciences, Institute for Chemical and Bioengineering, ETH Zurich, Wolfgang-Pauli-Strasse 10, 8093 Zurich, Switzerland
e-mail: hermans@chem.ethz.ch

B. Schimmöller
Department of Mechanical Engineering, Institute of Process Engineering, ETH Zurich, Sonneggstrasse 3, 8092 Zurich, Switzerland

conversion of two CyOOH molecules to one $CyOO^{\bullet}$ and one $CyO^{\bullet}$ radical [10–12]:

$$CyOOH + Co^{II} \rightarrow CyO^{\bullet} + Co^{III}\text{-}OH \quad (1)$$

$$CyOOH + Co^{III}\text{-}OH \rightarrow CyOO^{\bullet} + Co^{II} + H_2O \quad (2)$$

This catalytic cycle does not only decrease the CyOOH concentration, it also speeds up the rate-determining initiation reaction (i.e., the formation of radicals), explaining why the reaction temperature can be lowered. However, this simple mechanism fails to explain, for instance, why at higher cobalt concentrations, the reaction is inhibited. Indeed, a net decrease of the reaction rate is observed for $[Co^{II}] \geq 100$ μM under deperoxidation conditions [13]. A reasonable hypothesis is that at higher catalyst concentrations, cobalt dimers, or higher oligomers, are formed which efficiently destroy the peroxyl chain carriers. Currently, this hypothesis, as well as the influence of the ligand on the activity, selectivity and stability of this deperoxidation reaction, is under investigation.

However, the use of homogeneous deperoxidation catalysts causes several (technical) limitations. One of them is that the catalyst cannot be recycled and ends up in a high boiling waste stream. Another problem is that one is restricted to low catalyst concentrations in order to minimize contamination of the waste, and to prevent the deposition of cobalt to the stainless steel reactor walls. For these reasons, it would be of interest to develop a solid (heterogeneous) catalyst for this reaction. In the literature, a multitude of materials have already been proposed [e.g., 14–18], and providing an overview of all those systems would be beyond the scope of this paper. However, from a strategic (engineering) point of view, the following thoughts can be made. Many of the reported catalysts are high surface area materials, featuring active sites which are located in (micro/meso)-pores. Given the detrimental effect of mass-transfer limitation on the selectivity towards products which can react further (as is the case with desired partial oxidation products), and the increased polarity of the oxygenated products compared to the substrate, one can wonder if immobilization in micro-porous materials is an optimal approach. On the other hand, a high surface area is often required to achieve a high dispersion (accessibility) of the transition metal sites. One approach which some of us proposed a while ago is the immobilization of chromium hydroxy oxide colloids to the external surface of a silica support via a process called column-precipitation-chromatography (CPC) [19, 20]. This technique combines the synthesis of small particles with their in situ immobilization, preventing sintering. An alternative approach that we report in this paper, is the synthesis of nano-structured particles of cobalt-containing silica with flame-spray pyrolysis (FSP). FSP is a convenient technique to synthesize thermally stable materials with interesting properties as solid catalysts. Additional advantages of these materials is that they provide a high surface area without micro-pores, and that the synthesis is highly reproducible and scalable [21–24].

2 Experimental

2.1 Synthesis of the Nano-Structured Co/SiO_2 Particles

Nano-structured Co/SiO_2 particles were made by flame-spray-pyrolysis (FSP) of appropriate precursor solutions. Cobalt-2-ethylhexanoate (Co-2-ethylhexanoate, 12% Co, STREM Chemicals) and hexamethyldisiloxane (HMDSO, Aldrich, >98%) were used as cobalt and silicon precursors, respectively, dissolved in xylene (Riedel-de Haën, >96%) and 2-ethylhexanoic acid (Riedel-de Haën, >99%) in a ratio of 2:3, resulting in a total metal concentration of 1 mol L^{-1}. This precursor solution was fed by a syringe pump through the FSP nozzle and dispersed by O_2 (Pan-Gas, 99.95%, 5 L min^{-1}) into a fine spray that was ignited and sustained by a premixed CH_4/O_2 flame. Additional 5 L min^{-1} of sheath O_2 was fed in the reactor through a metal ring (11 mm internal diameter, 18 mm outer diameter) with 32 holes (0.8 mm internal diameter) to ensure complete combustion. A detailed description of the laboratory scale FSP reactor can be found elsewhere [25]. The powders were collected with the aid of a vacuum pump (Busch SV 1050 B) on a glass microfiber filter (Whatman GF/D, 257 mm in diameter).

2.2 Characterization

The specific surface area (m^2 g^{-1}) of the materials was determined by nitrogen adsorption (Pan Gas, >99.999%) at 77 K by the Brunauer–Emmett–Teller (BET) method with a Micromeritics Tristar 3000 (five point-isotherm, $0.05 < p/p_0 < 0.25$). The Co-loading of the material was determined with ICP-OES (Horiba, Ultima 2) after digestion with HF and found in fair agreement with the composition of the precursor solution. Raman spectra were recorded with a Renishaw InVia Raman microscope with a 514 nm laser excitation (±1 mW). Infrared spectra were recorded with a Bruker Vertex 70 V spectrometer (LN-MCT Mid detector) in a Pike Miracle® Attenuated Total Reflection (ATR) cell with a diamond crystal, or with a Bruker Alpha-P FT-IR spectrometer equipped with a diffuse reflectance module (DRIFT) mounted inside a glove-box; KBr was taken as background for the DRIFT spectra. Diffuse Reflectance UV–Vis spectra were recorded with an Ocean Optics Maya 2000Pro spectrometer with a

backscatter probe; in order to obtain Kubelka–Munk values below 1 and reproducible reflectivities, the samples were diluted in $BaSO_4$ as mentioned in the text and measured against a $BaSO_4$ background.

2.3 Catalytic Experiments

The experiments were performed at 130 °C in a 100 mL 316 stainless steel autoclave, equipped with an inert Polyether Ether Ketone (PEEK) insert, including a PEEK top lid, PEEK stirrer and a PEEK covered thermocouple. The short heating time (15 min) and the accurate temperature control ensured stable conditions during the reaction. After loading the reactor with catalyst and cyclohexane (30 mL), 400 psi (i.e., 27.6 bar) of oxygen pressure (Pan-Gas 99.999 vol.%) was added to the reactor, prior to heating. Notice that a potentially explosive gas-mixture is formed. Therefore, the reactor vessel was connected to a steel expansion vessel of 20 L via a rupture disk, designed to open at 150 bar. The pressure in the reactor was monitored with a pressure gauge and a pressure sensor (Keller), connected to a computer. Slurry samples were withdrawn from the reactor via a PEEK sampling tube and analyzed by GC (HP6890; HP-5 column, 30 m/0.32 mm/0.25 mm; Flame Ionization Detector). Biphenyl was added to the cyclohexane in 0.25 mol.%, and used as an inert internal standard for product quantification. In order to ensure that all insoluble/adsorbed by-products were also quantified, the withdrawn samples were centrifuged, the solid catalyst washed 3× with acetone, and the solutions combined. The O–H groups in the reaction mixture were silylated with *N*-Methyl-*N*-(trimethylsilyl)trifluoroacetamide (MSTFA) to facilitate the separation of the alcohol and the ketone product; note that the acidic by-products such as adipic and glutaric acid are also silylated by MSTFA. The hydroperoxide yield was determined via a double injection into the GC, with and without reduction of the reaction mixture by trimethylphosphine (Sigm-Aldrich, 1 M in toluene), prior to silylation. From the obtained augmentation in alcohol content, the corresponding hydroperoxide yield was determined. Product identification was done with GC–MS with cool-on-column injection to prevent thermal dissociation in the GC-liner.

3 Results and Discussion

3.1 Autoxidation Experiments

It is important to realize that the reactor wall can have a significant effect on the observed activity and selectivity during lab-scale studies of oxidation reactions, due to the catalytic decomposition of the hydroperoxides, either by the reactor wall itself, or by leached metal ion species. This effect, accelerating the autoxidation rate and reducing the hydroperoxide selectivity, makes it difficult to record the correct background activity and selectivity of autoxidations. Not only for autoxidations, but actually for every peroxide-based oxidation reaction, such as epoxidations with H_2O_2, this catalytic wall effect can cause serious problems. Indeed, a Fenton-type decomposition of the peroxide on the reactor wall will not only reduce the peroxide efficiency and the overall selectivity (viz. the initiation of side-reactions upon the formation of undesired radicals), it can also cause a safety issue as such decomposition reactions form O_2 which can build explosive gas-mixtures in the reactor. Moreover, a catalytic contribution of the reactor wall will also cause scale-up problems as the reactor surface-to-volume-ratio is inversely proportional to the reactor radius. Large scale industrial reactors are therefore much less subjective to such wall effects than small lab reactors. The design and correct operation of a reliable and robust laboratory set-up is therefore of great importance.

Although not generally acknowledged, peroxide solutions are intrinsically very stable, even at elevated temperatures. For example, in our hands, a 3 M aqueous H_2O_2 solution remains stable for more than 36 h at 80 °C in a carefully cleaned glass reactor. However, several materials used to construct reactors or reactor inserts cause peroxide decomposition. In order to get a more quantitative feeling for this decomposition activity, small cylindrical samples of various materials (surface area = 300 mm^2, volume = 550 mm^3) were placed in a 5 mL solution of a 3 M H_2O_2 solution in parallel glass reactors. These materials were: (1) Polyaryl Ether Ether Ketone (PEEK), (2) Teflon®, (3) pre-passivated aluminium, (4) stainless steel SS316, and (5) titanium. Visual inspection of the solutions shows the following reactivity towards H_2O_2 decomposition: PEEK $\ll$ Teflon® $<$ SS316 $<$ Al $<$ Ti. A permanganometric titration versus a sodium oxalate standard confirmed those results: the H_2O_2 decomposition after 8 h equals: <5% for PEEK, 25% for Teflon®, 30% for SS316, 40% for Al, 70% for Ti. The reason why an inert polymer such as Teflon® seems to decompose H_2O_2 is at the moment not fully clear. The hypothesis that un-reacted monomer species (still containing reactive C=C bonds) would be responsible for this behavior seems to be in disagreement with the steady activity over several hours. This observation points more in the direction of H-bond activated dissociation of the H_2O_2 as previously suggested for μm Teflon® particles [26]. Also remarkable is the significant activity of the aluminium sample. Prior to its testing, the Al sample was subsequently contacted with H_2O_2/HNO_3 solutions of increasing concentration to remove traces of iron, remaining from the manufacturing process (machining) and to form a passivated Al_2O_3 layer. After several steps, the Al insert obtains indeed

a non-glossy white color, indicating the formation of a passivated Al_2O_3 layer. The thickness of this layer was further extended by treating the material for 48 h in 50 wt% H_2O_2 at room temperature. The stainless steel sample was significantly more active than PEEK and Teflon®. This is important as most of the commercial high-pressure reactors are constructed out of stainless steel. Interesting to note is that the activity decreases upon subsequent H_2O_2 treatments. This observation points to a self-passivation mechanism which probably involves leaching of weakly surface-bonded metal (ions), leaving behind a clean surface. The Ti sample was found to be by far the most active H_2O_2 decomposition catalyst. In solution one observes a colloidal dispersion, probably TiO_2 particles. These screening results show that even materials which one would expect to be completely inert are active in the (undesired) decomposition of peroxides. This implies that whenever performing peroxide based oxidations one should carefully investigate the contribution of the reactor, especially when working in a small scale.

The autoxidation of cyclohexane is very sensitive to this sort of wall effect. Earlier, it was reported that stainless steel reactors can be passivated by contacting the metal with a saturated solution of sodium pyrophosphate [4]. However, it is important to emphasize that the reactor only becomes completely passivated after a very long time (i.e., many subsequent runs of passivation and oxidation reactions). Even ppb amounts of Fenton-active ions, like iron or chromium, are able to modify the activity and selectivity during the autoxidation of cyclohexane. Especially the cyclohexanol over cyclohexanone ratio (ol/one) is very sensitive to metal catalyzed deperoxidations. An important problem is that neither the background activity of the reactor wall, nor the obtained selectivity is reproducible before the reactor is completely passivated. Similar effects were observed in reactors constructed from Hastelloy B and C.

In order to reduce the reactivity of the reactor wall, and/or to prevent leaching of metal ions, we evaluated the possibility of coating the steel with Teflon®. Three different layers of coating were subsequently applied: (i) a ground layer providing a rough sticky basic layer, (ii) an intermediate connecting layer, mainly consisting of Teflon®-Perfluoro-Alkoxy (PFA), followed by (iii) a last layer of Teflon® and cured at 410 °C for 6 min. Such a coating is routinely applied in cooking pans, but also in chemical storage tanks to make them inert towards aggressive chemicals. This approach resulted in a significant reduction of the reactivity and a remarkable improvement in the ol/one ratio. Unfortunately, the inert Teflon® layer was found to come off the wall after a few runs.

Because of the promising results with the Teflon® coating, we decided to explore the possibility of using a Teflon® insert (wall thickness 2.5 mm). Although this insert acts as an insulating barrier, resulting in an increased heating time, the cyclohexane autoxidation results were reasonable. Despite the good CyOOH selectivity, the ol/one ratio was still significantly lower than expected and not reproducible. A similar effect was observed earlier with micrometer Teflon® particles and attributed to a catalyzed conversion of the cyclohexylhydroperoxide to cyclohexanone [26]. Of all materials tested in the decomposition of H_2O_2, the thermoplastic PEEK (Polyaryl Ether Ether Ketone) showed the least activity (vide supra). This material is often used as an inert material with excellent mechanical strength and a lower porosity than for instance Teflon®. Cyclohexane autoxidation experiments were indeed very reproducible in PEEK inserts (see Experimental), resulting in a high CyOOH selectivity (around 80% at 2% conversion) and an ol/one ratio $\geq$1.5 (Fig. 1).

It has to be emphasized that the by-products plotted in Fig. 1 only refer to the sum of the most important by-products: 6-hydroxyhexanoic acid, 6-hydroperoxyhexanoic acid, adipic acid, glutaric acid and ε-caprolactone. However, several other (low boiling point) by-products are additionally formed (e.g., valeric acid, methanol, 1-butanol, 1-pentanol, CO, CO_2, …), especially at higher concentrations. Figure 2 shows how the selectivity depends on the conversion if both the liquid and the gas phase is thoroughly analyzed.

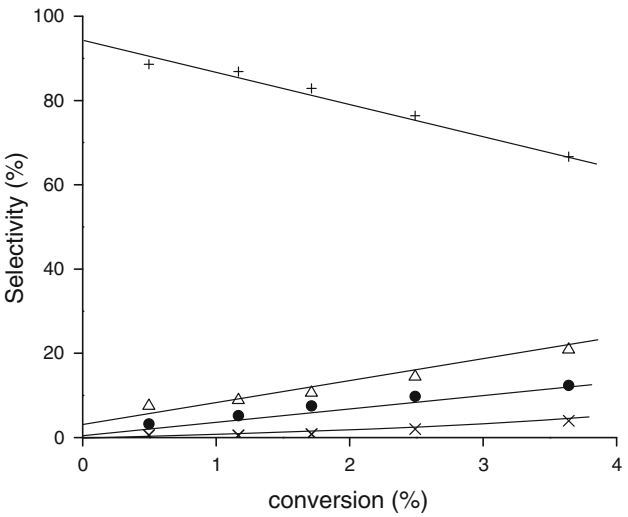

Fig. 1 Product distribution obtained during a pure autoxidation experiment at 145 °C: CyOOH (*plus*), CyOH (*open triangle*), Q=O (*filled circle*) and by-products (*cross*, sum of 6-hydroxyhexanoic acid, 6-hydroperoxyhexanoic acid, adipic acid, glutaric acid and ε-caprolactone)

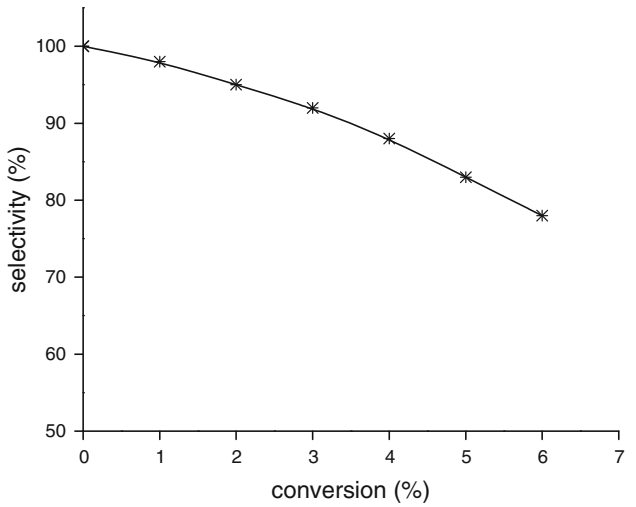

Fig. 2 Evolution of the overall selectivity versus the conversion for a thoroughly analyzed cyclohexane autoxidation system

3.2 Flame-Made Co/SiO_2

Using flame spray pyrolysis (FSP), Co/SiO_2 materials were synthesized with various amounts of cobalt, ranging from 3.4 to 7.6 wt%. Previously, the FSP method was demonstrated to be very reproducible [27]. The actual Co content, measured by ICP-OES after digestion with HF, and the BET surface areas of the materials are summarized in Table 1.

Flame-made silica particles from turbulent, vapor-fed flames are known to have an agglomerate size of around 10–300 nm [28], the structure of the agglomerates being very fractal (D_f around 2.1) [29]. FSP-made silica-based materials usually show a type IV isotherm with a very small hysteresis loop and possess no micro- or mesoporosity as seen for Pt/SiO_2 [27] and V_2O_5/SiO_2 [30] catalysts. Doping silica with Co has a pronounced effect on the specific surface area: starting from around 270 $m^2\ g^{-1}$ for pure FSP-made SiO_2 (not shown), the surface area initially increases for the 3.4 wt% sample up to around 330 $m^2\ g^{-1}$. Increasing the Co content further decreases the specific surface area even below the value of pure SiO_2. A similar trend of maximum specific surface area at low dopant content has already been observed previously for FSP-made Ta_2O_5/SiO_2 [31], V_2O_5/SiO_2 [30], ZnO-containing SiO_2 [32–35] and $Cs_2O/Pt/Al_2O_3$ [27]. In these studies it was shown by means of ammonia Temperature Programmed Desorption (TPD) that the particle surface is enriched with the doping element and is significantly different from pure FSP-made silica [31] or alumina [30], respectively. Therefore, the initial increase in surface area (i.e., from 270 to 330 $m^2\ g^{-1}$ for 0–3.4 w% cobalt) could be related to an influence of the cobalt constituent on the SiO_2 sintering rate and corroborates Co enrichment on the particle surface rather than incorporation in the bulk. The subsequent decrease in surface area at higher Co contents may be attributed to a segregation of CoO_x-clusters reducing the effect on the sintering rate and leading to larger primary particles and at higher contents, segregation of the dopant-metal-oxide reducing the overall specific surface area as observed for Ta_2O_5/SiO_2 [31] and V_2O_5/SiO_2 [30].

Table 1 Specific surface area of the various FSP-made Co/SiO_2 materials

Entry	Catalyst loading (wt%)[a]	Specific surface area according to BET ($m^2\ g^{-1}$)
a	3.4	330
b	4.8	300
c	5.6	270
d	7.6	220

[a] Determined by ICP-OES after complete digestion in HF (absolute error margin estimate at ±1%)

The UV–Vis Diffuse Reflectance (DRS) measurements of the different materials are reported in Fig. 3. Around 600 nm, one observes the typical triplet band, characteristic for isolated, tetrahedrally coordinated Co^{II} (assigned to the $^4A_2(F) \rightarrow {}^4T_1(P)$ transition) [36]. In addition, one observes an increased intensity around 400–550 nm for the 7.6 wt% sample, probably due to octahedrally coordinated cobalt ions [34–36]. (As a comparison, Fig. 3 also shows the DRS spectra of Co_3O_4 and CoO.) Note that the prominent presence of tetrahedral Co^{II} species corroborates the surface enrichment hypothesis as incorporation of cobalt in the silica bulk would require charge compensating cations like protons being incorporated in the bulk silica (viz. substitution of Co^{II} for Si^{IV}).

Diffuse Reflectance Infrared Fourier Transform (DRIFT) spectroscopy shows a broad band corresponding to hydrogen-bonded silanol vibrations around 3560 cm^{-1} and a sharp peak at 3740 cm^{-1} corresponding to isolated SiOH surface species; both signals decrease at increasing Co-loadings, indicating that the cobalt influences the silica surface significantly. IR spectroscopy also reveals that no residual organic species can be found on the fresh materials (which could originate from incomplete combustion of the precursor solution) (Fig. 4).

Raman spectroscopy shows several features (Fig. 5), and the most significant change is the growing signal at ±680 cm^{-1} with increasing Co-loadings, probably due to the formation of cobalt oxides at increasing loadings. This observation is consistent with the DRS spectra in Fig. 3, providing evidence for octahedrally coordinated species at higher Co-loading and corroborates the hypothesis of CoO_x segregation from BET analysis (vide supra). However, as the extinction coefficient of octahedral cobalt is lower than

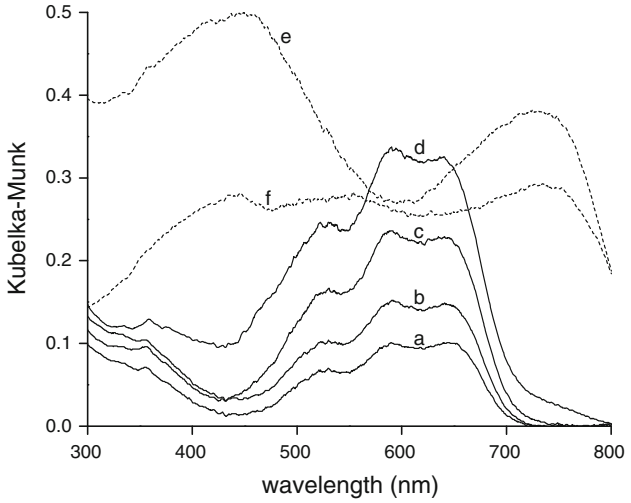

Fig. 3 DRS spectra of the FSP-made Co/SiO_2 samples (*a–d*, see Table 1; diluted 1:9 in $BaSO_4$), and of Co_3O_4 (*e*) and CoO (*f*; diluted 1:40 and 1:8, respectively, in $BaSO_4$)

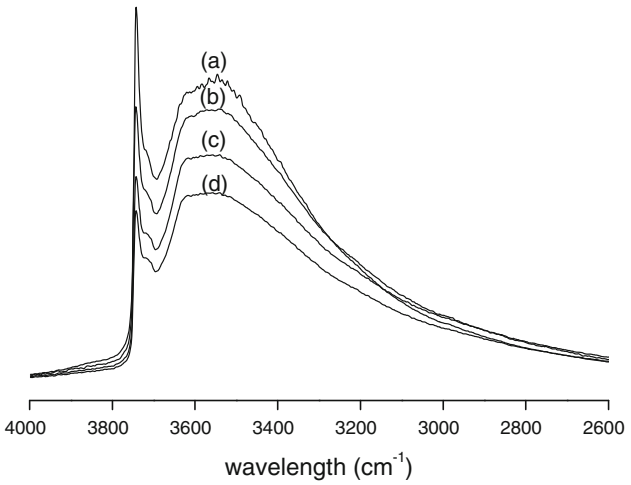

Fig. 4 DRIFT spectra of the different Co/SiO_2 samples (*a–d*, see Table 1)

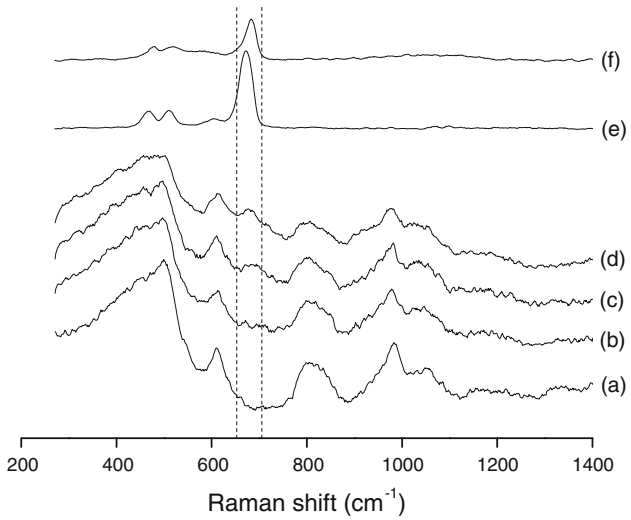

Fig. 5 Raman spectra of the different Co/SiO_2 materials (*a–d*, see Table 1), Co_3O_4 (*e*) and CoO (*f*)

of tetrahedral cobalt (d–d transitions are symmetry forbidden) [34–36], those higher coordinated species are barely visible with UV–Vis spectroscopy.

Summarizing the characterization results, one can conclude that cobalt is predominantly present as isomorphously substituted Co^{II}-ions in a tetrahedral environment, mainly on the particle surface. Only at high Co-loadings, octahedrally coordinated cobalt species are detected with UV–Vis and Raman spectroscopy, presumably present as very small cobalt oxides.

3.3 The Catalytic Performance

The performance of the FSP-made Co/SiO_2 materials as a catalyst for cyclohexane oxidation was studied at 130 °C under 400 psi (i.e., 27.6 bar) pure oxygen (room temperature pressure, i.e., prior to heating). Under those conditions, the thermal (i.e., the un-catalyzed) activity is negligible in the investigated timeframe. The catalytic activity (Fig. 6) appears to be significantly higher than that of commercially available Co_3O_4 nano-particles (Sigma-Aldrich, size < 50 nm), and much higher than the activity of the uncatalyzed system. To our initial surprise, the activity and selectivity are nearly independent of the Co-loading (see for instance Fig. 6). This effect can either be due to a constant amount of accessible and catalytically active sites at the surface of the materials, independent of the Co-loading, or, and more probable, due to a saturation effect. It was indeed observed that 5 ppm of the 3.4 wt% Co/SiO_2 performed equally well as 25 ppm of the same material. Apparently, once a critical amount of active Co-sites is present, further increase of the catalyst concentration does not increase the performance. It is possible that a change in rate-determining-step from CyOOH coordination/diffusion to the Co-sites to the actual decomposition at the active site, is behind this observation. However, more kinetic experiments are required to verify this hypothesis.

Of practical interest is the very low CyOOH selectivity (Fig. 7), compared to the thermal autoxidation (Fig. 1).

Figure 8 shows the selectivity as a function of the conversion for a cyclohexane oxidation, catalyzed by 5 ppm Co(II) acetylacetonate—$Co(acac)_2$—which features a similar activity as the reported heterogeneous systems [9]. However, the use of such a high concentration of a homogeneous catalyst is technically prohibited (see Introduction). Remarkable is that the heterogeneous catalyst results in a higher CyOH yield, due to a more complete

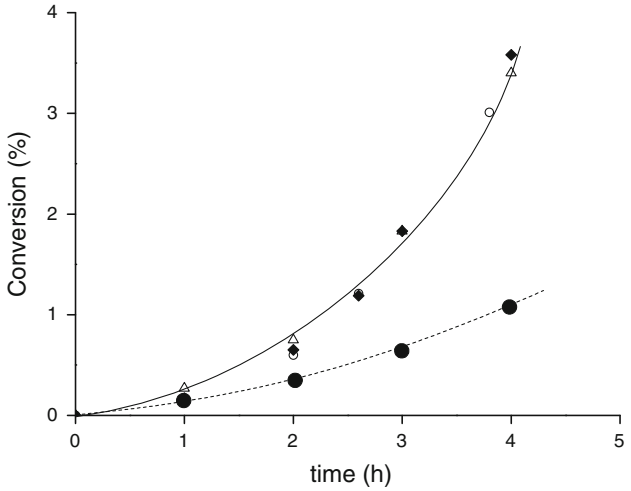

Fig. 6 Evolution of the cyclohexane conversion as a function of time at 130 °C using 25 mg L^{-1} cobalt, using various catalysts: 3.4 wt% Co/SiO_2 (*filled diamond*), 4.8 wt% Co/SiO_2 (*open circle*), 7.6 wt% Co/SiO_2 (*open triangle*), and Co_3O_4 nano-particles (*filled circle*, <50 nm, Sigma-Aldrich)

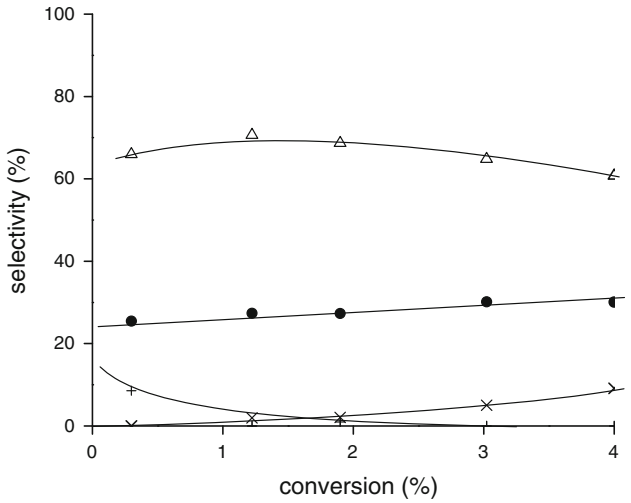

Fig. 7 Product distribution obtained during a catalytic cyclohexane oxidation experiment at 130 °C, using 25 ppm of a 3.4 wt% Co/SiO_2 sample: CyOOH (*plus*), CyOH (*open triangle*), Q=O (*filled circle*) and by-products (*cross*, sum of 6-hydroxyhexanoic acid, 6-hydroperoxyhexanoic acid, adipic acid, glutaric acid and ε-caprolactone)

deperoxidation. Possibly this can be attributed to sorption effects, increasing the local CyOOH concentration near the catalytic sites.

3.4 Coordination of Hydroperoxide

When the catalyst is impregnated with a 100 mM *t*-butylhydroperoxide solution (diluted in cyclohexane), the broad triplet band around 600 nm in the DRS spectrum decreases

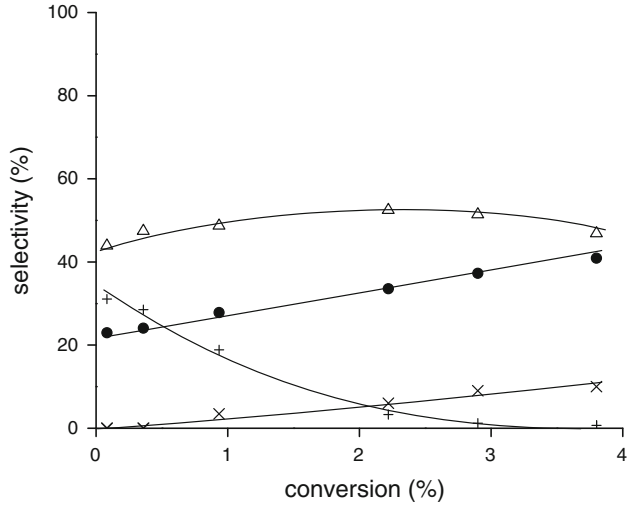

Fig. 8 Product distribution obtained during a catalytic cyclohexane oxidation experiment at 130 °C, using 5 ppm of $Co(acac)_2$: CyOOH (*plus*), CyOH (*open triangle*), Q=O (*filled circle*) and by-products (*cross*, sum of 6-hydroxyhexanoic acid, 6-hydroperoxyhexanoic acid, adipic acid, glutaric acid and ε-caprolactone)

significantly in intensity (Fig. 9). (The increased UV-signal can be attributed to the absorption by the hydroperoxide itself.) Note that this observation supports the hypothesis that the tetrahedral Co^{II} species are located at the surface of the material, accessible for reactants. Indeed, probably this means that the hydroperoxide is coordinating, breaking the tetrahedral symmetry of the cobalt sites. More (in situ) spectroscopic work is required to verify if this observation implies that the active deperoxidation site is a $[CoO_4]$ surface-species.

3.5 Product Analysis and Desorption of By-Products

Important to emphasize here is the need for a quantitative product analysis [37]. Indeed, after a catalytic run, a lot of by-products such as adipic acid are adsorbed to the solid catalyst. Attenuate Total Reflection Infrared (ATR-IR) spectroscopy actually only detects adipic acid (Fig. 10). As a consequence, it is very easy to overestimate the selectivity. Indeed, in case of inhomogeneous sampling (i.e., only liquid is sampled, no solid material containing adsorbed by-products), or if the catalyst is not carefully washed with acetone to dissolve the by-products for correct product quantification (see Experimental), a much higher selectivity was observed, surpassing the current state-of-the-art (Fig. 2). The ATR-IR results in Fig. 9 show that the adipic acid can indeed be desorbed from the solid catalyst upon washing with acetone. This analytical procedure results in a similar overall selectivity towards the sum of desired products as the non-catalyzed thermal autoxidation reaction, however with a negligible contribution of CyOOH.

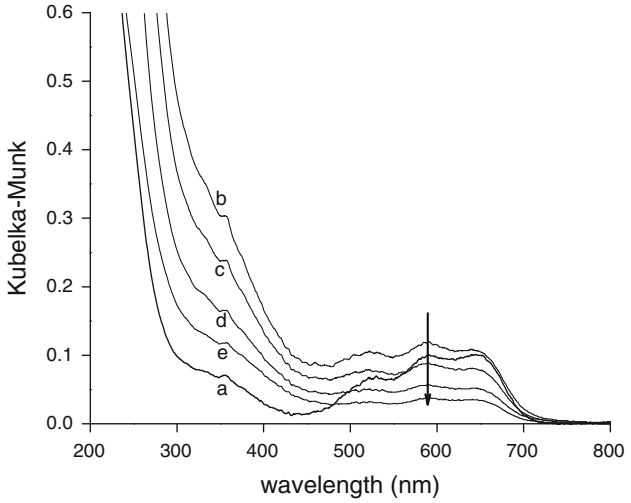

Fig. 9 DRS spectra of the 3.4 wt% FSP Co/SiO_2 material, before (*a*), and after (*b*) exposure to a 100 mM *t*-butylhydroperoxide solution; spectra (*c*–*e*) were recorded at 5 min time interval

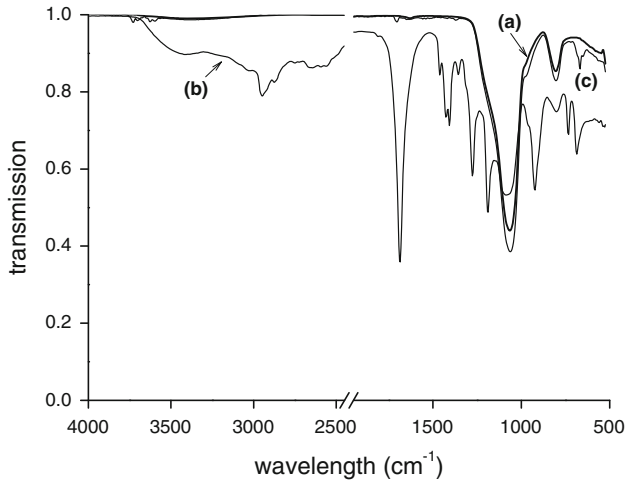

Fig. 10 Attenuated total reflection IR spectra of the 3.4 wt% Co/SiO_2 before a catalytic run (spectrum *a*), after a catalytic run (spectrum *b*), and after subsequent washing with acetone (3×, spectrum *c*)

3.6 Stability of the Catalyst: Hot Separation Test

A common problem encountered in liquid phase applications of solid catalysts is leaching of the active elements. Especially for (aut)oxidation reactions, leaching is a notorious issue [38]. One of the most robust lab-scale experiments to verify if leached species cause homogenous rather than heterogeneous catalysis, is the so-called hot-separation test. In this experiment, the supernatant is separated from the solid catalyst (e.g., by centrifugation), prior to cooling down of the reaction mixture. Indeed, the latter could induce re-adsorption or re-precipitation of leached species. Subsequently, the remaining activity of the

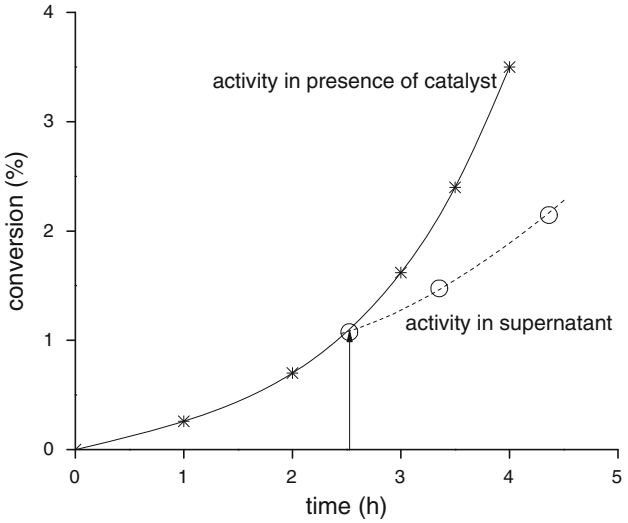

Fig. 11 Results of a hot-separation test at 130 °C: the solid catalyst (25 ppm, 3.4 wt% Co/SiO_2) is separated from the hot reaction mixture after 2.5 h and the conversion of supernatant monitored for an additional 2 h

supernatant devoid of catalyst is examined under the same conditions. In case that the catalysis is purely caused by leached species, the oxygenation activity of the supernatant would match the activity of the catalytic (slurry) system (under the assumption that there is no important support effect, boosting the activity). In our case, a hot reaction mixture containing the solid catalyst (3.4 wt% Co/SiO_2) was centrifuged after 2.5 h, and the oxidation of the supernatant was followed for another 2 h. As can be seen from Fig. 11, the conversion did continue to increase, albeit at a much lower rate. Previously, some of us observed very similar behavior in a hot-separation test of supported chromium nano-particles [19, 20]. The persistence of a low activity can be attributed to the thermal autoxidation, initiated by the oxygenated products, present in the supernatant [19, 20]. An important observation is that the CyOOH selectivity in the supernatant increases very rapidly, i.e., from nearly zero in the catalytic slurry system (see Fig. 7) to 20% in the supernatant test after 2 h of reaction (viz. at 2% conversion, see Fig. 11). This observation provides strong evidence to assume that no catalytically active amounts of cobalt are leached in solution as this would keep the CyOOH selectivity very low indeed. Similar results were observed if the hot-separation test was performed after 3.5 h. The cobalt concentration in the supernatant solution was also investigated by ICP-OES and found to be below the detection limit, implying that less than 1% of the cobalt could have leached out without noticing it.

Recycling of the FSP Co/SiO_2 catalyst has also been examined under the usual conditions (27.6 bar O_2, 130 °C). After a 4 h oxidation run, the solid catalyst (3.4 wt%,

25 ppm) was separated from the liquid phase and washed several times with acetone to remove adsorbed by-products (vide supra). Subsequently the solid was dried at 70 °C in a vacuum oven. The reaction rate with the recycled catalyst was slightly higher than with fresh catalyst, probably due to the presence of small amounts of organic products which were not completely removed upon washing (see Fig. 10, spectrum c). However, the two subsequent recycle experiments all showed the same steady activity. It is important to emphasize that the product distributions remained essentially the same during these recycle experiments. All these results hence point towards the heterogeneous nature of this FSP Co/SiO_2 catalyst.

4 Conclusions

Flame-spray-pyrolysis was used as a convenient technique to synthesize Co/SiO_2 materials with different loadings. At low loadings, the cobalt is mainly present as tetrahedral species at the surface of the particles. At higher loadings, also octahedral cobalt, probably (mixed) cobalt oxide, can be detected by DRS UV–Vis and Raman spectroscopy. The materials were demonstrated to be active autoxidation catalysts, affording very low hydroperoxide selectivity. This does not only improve the intrinsic safety of the oxidation process, but it also eliminates the need for a second, subsequent deperoxidation step. Emphasis is put on correct product analysis to study the intrinsic selectivity of the system; leaching of active cobalt species which could cause homogeneous rather than heterogeneous catalysis can be neglected, based on hot-separation and recycle experiments. In subsequent work, the long term stability of the catalyst under continuous flow conditions should be investigated.

Acknowledgments NT and IH acknowledge the financial contributions by the Swiss National Science Foundation (grant 200021_124698 2 and 206021_128688 3) and are grateful for the help from the company ILAG (Lachen, Switzerland) in coating high pressure reactors with Teflon®; BS is grateful for the financial support by ETH Research Grant TH-41 06-1. The authors thank Prof. Sotiris E. Pratsinis for useful discussions.

References

1. Sheldon RA, Kochi JK (1981) Metal catalyzed oxidations of organic compounds. Academic, New York
2. Schäfer R, Merten C, Eigenberger G (2003) Can J Chem Eng 81:741
3. Hermans I, Peeters J, Jacobs PA (2008) Top Catal 48:41
4. Hermans I, Nguyen TL, Jacobs PA, Peeters J (2005) Chem Phys Chem 6:637
5. Hermans I, Jacobs PA, Peeters J (2006) Chem Eur J 12:4229
6. Hermans I, Jacobs PA, Peeters J (2006) J Mol Catal A: Chem 251:221
7. Hermans I, Peeters J, Jacobs PA (2008) Top Catal 50:124
8. Hermans I, Jacobs PA, Peeters J (2007) Chem Eur J 13:754
9. Hermans I, Peeters J, Jacobs PA (2008) J Phys Chem A 112:1747
10. Tolman CA, Druliner JD, Nappa MJ, Herron N (1989) In: Hill CL (ed) Activation and functionalization of alkanes. Wiley, New York
11. Franz G, Sheldon RA (2000) Oxidation, Ullmann's encyclopedia of industrial chemistry. Wiley-VCH, Weinheim
12. Bhaduri S, Mukesh D (2000) Homogeneous catalysis, mechanisms and industrial applications. Wiley, New York
13. Turrà N, Neuenschwander U, Baiker A, Peeters J, Hermans I (2010) Chem Eur J 16:13226
14. Emanuel NM, Maizus ZK, Skibida IP (1969) Angew Chem Int Ed Engl 8:97
15. Vanoppen DL, De Vos DE, Genet MJ, Rouxhet PG, Jacobs PA (1995) Angew Chem Int Ed Engl 34:560
16. Nowotny M, Pedersen LN, Hanefeld U, Maschmeyer T (2002) Chem Eur J 8:3724
17. Ramanathan A, Hamdy MS, Parton R, Maschmeyer T, Jansen JC, Hanefeld U (2009) Appl Catal A Gen 355:78
18. Sankar G, Raja R, Thomas JM (1998) Catal Lett 55(1):15
19. Breynaert E, Hermans I, Lambie B, Maes G, Peeters J, Maes A, Jacobs PA (2006) Angew Chem Int Ed 45:7584
20. Hermans I, Breynaert E, Poelman H, De Gryse R, Liang D, Van Tendeloo G, Maes A, Peeters J, Jacobs PA (2007) Phys Chem Chem Phys 9:5382
21. Strobel R, Baiker A, Pratsinis SE (2006) Adv Power Technol 17:457
22. Strobel R, Pratsinis SE (2007) J Mater Chem 17:4743
23. Mueller R, Madler L, Pratsinis SE (2003) Chem Eng Sci 58:1969
24. Madler L, Kammler HK, Mueller R, Pratsinis SE (2002) Aerosol Sci 33:369
25. Schimmoeller B, Schulz H, Ritter A, Reitzmann A, Kraushaar-Czarnetzki B, Baiker A, Pratsinis SE (2008) J Catal 256:74
26. Hermans I, Jacobs PA, Peeters J (2006) Chem Phys Chem 7:1142
27. Schimmoeller B, Hoxha F, Mallat T, Krumeich F, Pratsinis SE, Baiker A (2010) Appl Catal A Gen 374:48
28. Wengeler R, Teleki A, Vetter M, Pratsinis SE, Nirschl H (2006) Langmuir 22:4928
29. Camenzind A, Schulz H, Teleki A, Beaucage G, Narayanan T, Pratsinis SE (2008) Eur J Inorg Chem 6:911
30. Schimmoeller B, Jiang YJ, Pratsinis SE, Baiker A (2010) J Catal 274:64
31. Schulz H, Madler L, Pratsinis SE, Moszner N (2005) Adv Funct Mater 15:830
32. Tani T, Madler L, Pratsinis SE (2002) J Mater Sci 37:4627
33. Ashley JH, Mitchell PCH (1968) J Chem Soc 2821
34. Verberckmoes AA, Weckhuysen BM, Schoonheydt RA (1998) Microporous Mesoporous Mater 22:165
35. Weckhuysen BM, Rao RR, Martens JA, Schoonheydt RA (1999) Eur J Inorg Chem 565
36. WeckhuysenBM, Schoonheydt RA (2000) In: Weckhuysen BM, Van Der Voort P, Catana G (eds) Spectroscopy of transition metal ions on surfaces. Leuven University Press, Leuven
37. Hereijgers BPC, Weckhuysen BM (2010) J Catal 270:16
38. Sheldon RA, Wallau M, Arends IWCE, Schuchardt U (1998) Acc Chem Res 31:485